Full-color three-dimensional microscopy by wide-field optical coherence tomography

Lingfeng Yu and M.K. Kim

Dept. of Physics, University of South Florida, Tampa, FL 33620
mkkim@cas.usf.edu

Abstract: We demonstrate a method of optical tomography for surface and sub-surface imaging of biological tissues, based on the principle of wide field optical coherence tomography and capable of providing full-color three-dimensional views of a tissue structure. Contour or tomographic images are obtained with an interferometric imaging system using broadband light sources. The interferometric images are analyzed in the three color channels and recombined to generate 3D microscopic images of tissue structures with full natural color representation. In contrast to most existing three-dimensional microscopy methods, the presented technique allows monitoring of tissue structures close to its natural color, which may be useful in physiological and pathological applications.

OCIS codes: (180.6900) Three-dimensional microscopy; (110.4500) Optical coherence tomography;

References and links

1. C.J.R. Sheppard and D.M. Shotton, *Confocal Laser Scanning Microscopy*, (Springer, New York, 1997).
2. A.F. Fercher, W. Drexler, C.K. Hitzenberger, and T. Lasser, "Optical coherence tomography – principles and applications," Rep. Prog. Phys. **66**, 239-303 (2003).
3. F.M. Xu, H.E. Pudavar, P.N. Prasad, and D. Dickensheets, "Confocal enhanced optical coherence tomography for nondestructive evaluation of paints and coatings," Opt. Lett. **24**, 1808-1810 (1999).
4. Z. Ding, Y. Zhao, H. Ren, J.S. Nelson, and Z. Chen, "Real-time phase-resolved optical coherence tomography and optical Doppler tomography," Opt. Exp. **10**, 236-245 (2002), http://www.opticsexpress.org/abstract.cfm?URI=OPEX-10-5-236.
5. E.A. Swanson, J.A. Izatt, M.R. Hee, D. Huang, C.P. Lin, J.S. Schuman, C.A. Puliafito, and J.G. Fujimoto, "In vivo retinal imaging by optical coherence tomography," Opt. Lett. **18**, 1864-1866 (1993).
6. C.K. Hitzenberger, P. Trost, P.W. Lo, and Q. Zhou, "Three-dimensional imaging of the human retina by high-speed optical coherence tomography," Opt. Exp. **11**, 2753-2761 (2003), http://www.opticsexpress.org/abstract.cfm?URI=OPEX-11-21-2753.
7. P.J. Smith, C.M. Taylor, A.J. Shaw, and E.M. McCabe, "Programmable array microscopy with a ferroelectric liquid-crystal spatial light modulator," Appl. Opt. **39**, 1664-1669 (2000).
8. M. A. A. Neil, R. Juskaitis, and T. Wilson, "Method of obtaining optical sectioning by using structured light in a conventional microscope," Opt. Lett. **22** 1905-1907 (1997).
9. E. Bordenave, E. Abraham, G. Jonusauskas, N. Tsurumachi, J. Oberle, C. Rulliere, P. E. Minot, M. Lassegues, and J.E.S. Bazeille, "Wide-field optical coherence tomography: imaging of biological tissues," Appl. Opt. **41**, 2059-2064 (2002).
10. B. Laude, A. De Martino, B. Drevillon, L. Benattar, and L. Schwartz, "Full-field optical coherence tomography with thermal light," Appl. Opt. **41**, 6637-6645 (2002).
11. A. Dubois, L. Vabre, A.C. Boccara, and E. Beaurepaire, "High-resolution full-field optical coherence tomography with Linnik microscope," Appl. Opt. **41**, 805-812 (2002).
12. M. Ducros, M. Laubscher, B. Karamata, S. Bourquin, T. Lasser, and R. P. Salathe, "Parallel optical coherence tomography in scattering samples using a two-dimensional smart-pixel detector array," Opt. Comm. **202**, 29-35 (2002).
13. M.K. Kim, "Tomographic three-dimensional imaging of a biological specimen using wavelength-scanning digital interference holography," Opt. Exp. **7**, 305-310 (2000), http://www.opticsexpress.org/abstract.cfm?URI=OPEX-7-9-305.
14. A. Dakoff, J. Gass, and M.K. Kim, "Microscopic three-dimensional imaging by digital interference holography," J. Electronic Imaging **12**, 643-647 (2003).

#5639 - $15.00 US Received 3 November 2004; revised 14 December 2004; 16 December 2004

15. Y. Sando, M. Itoh, and T. Yatagai, "Color computer-generated holograms from projection images," Opt. Exp. **12**, 2487-2493 (2004), http://www.opticsexpress.org/abstract.cfm?URI=OPEX-12-11-2487.
16. I. Yamaguchi, T. Matsumura, and J.I. Kato, "Phase-shifting color digital holograph," Opt. Lett. **27**, 1108-1110 (2002).

1. Introduction

One of the main thrust areas of the development of modern microscopy is three-dimensional microscopy, where one acquires three-dimensional image with every image plane sharply in focus. This is in contrast to conventional microscopy where the image of in-focus plane is superposed with blurred image of out-of-focus planes. In confocal scanning microscopy (CSM) [1], the out-of-focus signal is spatially filtered out by confocal aperturing of the object illumination and the detector points. The three-dimensional image is constructed by pixel-by-pixel mechanical scanning of the entire object volume, which places a fundamental limit on the image acquisition speed. Another more recent development in 3D microscopy is the optical coherence tomography (OCT) [2], where the axial resolution of a few μm is provided by interferometric measurement of the time-of-flight of short-coherence light. In a typical arrangement, a Michelson-type interferometer is illuminated by femtosecond laser or superluminescent LED, and the reference arm is dithered to generate a heterodyne signal in the interference with the back-scattered light from the sample point. The two- or three-dimensional image is constructed from the mechanical scanning over the sample area or volume, as in the confocal scanning microscopy. In order to maintain high speed of z-scan, considerably large depth of field, a mm or so, is needed, which compromises the lateral resolution to a few μm. A confocal adaptation [3] can be used to improve the resolution. The heterodyne detection allows very high sensitivity and unique capabilities such as Doppler velocity detection of blood flow [4]. The OCT-based imaging systems are being developed for diverse areas of medical imaging including retinal structures [5,6], endoscopy of gastrointestinal tract and catheter-based intravascular imaging. As a coherent imaging technique, the OCT is capable of penetrating a larger distance into highly scattering media such as biological tissues and ceramics. Scanning microscopies, including the confocal microscopy and optical coherence tomography, have a number of distinct advantages such as relaxed requirement on the imaging optics and high sensitivity and high resolution achievable. On the other hand, the mechanical scanning is a major limiting factor in the image acquisition speed. Parallel acquisition of two-dimensional images while maintaining the optical sectioning characteristics of CSM or OCT would have obvious advantages. In CSM, such 2D imaging is approximated with a large number of well-spaced apertures, such as rotating Nipkow disk or multi-aperture scanning using an electro-optic spatial light modulator [7], but the light efficiency or image contrast tends to be low. Wide field optical sectioning is also achieved by structured light microscopy where a moving grating pattern illuminates the object and processing of several images extracts the in-focus sectioned image [8].

With the OCT, full-field interferometric images can be acquired using broadband light source, and the regions of the image that do contain interferometric information can be extracted by digital processing of the CCD images, thus generating optical section images variously known as wide-field, full-field, or two-dimensional OCT [9,10]. The 3D image is constructed by mechanical scanning of axial direction only. A quasi-lock-in image acquisition [11] has been demonstrated using synchronous illumination, instead of synchronous detection, due to the limited frame rate of CCD camera, 30Hz. High-frequency, 50kHz, true lock-in image acquisition has also been demonstrated using custom made smart array detector [12], although with limited number of pixels, 58x58. These experiments have demonstrated the potential for high-speed high-resolution 3D microscopy with very respectable sensitivity or dynamic range, at least ~80db, and promise to have significant impact on OCT applications where acquisition speed is critical, as in real time in vivo ophthalmic and endoscopic imaging. Another 3D microscopy technique we have been developing recently is the digital

#5639 - $15.00 US Received 3 November 2004; revised 14 December 2004; 16 December 2004

interference holography (DIH), where holographic images of an object volume are numerically constructed from a set of holograms recorded with a series of wavelengths. The numerical superposition of all the image volumes results in a synthesized short coherence length and corresponding axial resolution [13,14].

Unlike conventional microscopy, most of the current developments of 3D microscopy usually discard the natural color information of the object, whereas in some of the critical application areas of OCT such as ophthalmic and dermatological imaging, the color and texture of relatively thin top layers of the tissues can provide vital information in a format that is familiar to medical specialists in these areas. In this paper we propose and demonstrate full-color 3D microscopic imaging by WFOCT (wide-field optical coherence tomography) using three color LED's. The WFOCT imaging is performed on an object three times using red, green, and blue LED's, and the resulting three RGB channels of the 3D images are combined to generate a final 3D image with full natural color representation. The RGB combination of three-channel imaging has been demonstrated in computer-generated holography (CGH) [15] and digital holography [16].

Below, we describe the general principles of color 3D microscopy by wide-field optical coherence tomography and present some experimental images. The paper concludes with a discussion of the results and future directions.

2. Full-color wide-field optical coherence tomography

The principle of color 3D microscopy by WFOCT is described referring to the diagram of apparatus in Fig. 1. A high-brightness LED (~30 lumens) illuminates the Michelson interferometer through a collimating lens L1, a polarizer P, and the broadband polarizing beam splitter BS. The quarterwave plates Q1 and Q2 in the object or reference arms change the orthogonal polarization states, so that all of the reflections from the object or the reference mirror are steered toward the monochrome CCD camera (Sony XC-ST50) through the imaging lens L2. The analyzer A combines the two beams into a common polarization to effect the interference between them. The combination of the polarizer and the analyzer allows continuous adjustment of the relative intensity and the interference contrast between the object and reference beams. The CCD image is acquired by the computer using an image acquisition board (National Instruments IMAQ PCI-1407) and a function generator (SFG) is used to strobe the LED and to dither the reference mirror mounted on a piezo-transducer (PZT). The object is mounted on a three-axis micrometer translation stage to bring appropriate object plane into focus.

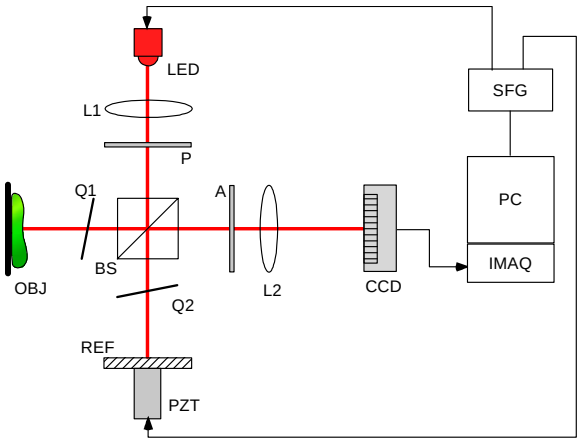

Fig. 1. Apparatus for color WFOCT. See text for details.

#5639 - $15.00 US Received 3 November 2004; revised 14 December 2004; 16 December 2004

The reference mirror is positioned at an equal distance with respect to the object focal plane within the coherence length of the LED, and the object contour is imaged by phase-shift interferometry. The light intensity distribution $I(x,y)$ on the CCD array is written as:

$$I = I_O(x,y) + I_B(x,y) + I_R(x,y) + 2\sqrt{I_O(x,y)I_R(x,y)}\cos[\varphi_i + \varphi(x,y)] \qquad (1)$$

where $I_O(x,y)$ is the portion of the object reflection that is coherent with respect to the reference $I_R(x,y)$ and $I_B(x,y)$ is the incoherent background. $\varphi(x,y)$ is the relative phase profile between the object and the reference beams, whereas φ_i is the phase shift introduced by the piezo-driven reference. The reference mirror is dithered by a sawtooth wave applied to the reference piezo mount over a few micron amplitude. Four image frames are acquired at quarter wavelength intervals corresponding to reference phases of $\varphi_i = 0$, $\pi/2$, π, and $3\pi/2$. These interference images are expressed as:

$$\begin{aligned} I_0 &= I_O + I_B + I_R + 2\sqrt{I_O I_R}\cos\varphi \\ I_{\pi/2} &= I_O + I_B + I_R - 2\sqrt{I_O I_R}\sin\varphi \\ I_\pi &= I_O + I_B + I_R - 2\sqrt{I_O I_R}\cos\varphi \\ I_{3\pi 2} &= I_O + I_B + I_R + 2\sqrt{I_O I_R}\sin\varphi \end{aligned} \qquad (2)$$

The amplitude of the coherent object image is then given by

$$I_O = \frac{(I_0 - I_\pi)^2 + (I_{\pi/2} - I_{3\pi/2})^2}{16 I_R} \qquad (3)$$

and the phase map

$$\varphi = \tan^{-1}\frac{I_{3\pi/2} - I_{\pi/2}}{I_0 - I_\pi} \qquad (4)$$

In Fig. 2, we use a plane mirror as the object, tilted by a small angle with respect to the optical axis. The four interference images show that the fringes are shifted by quarter periods. The interference profiles are also plotted in Fig. 2. The bottom image and curve show the envelope of the interference profile as obtained by Eq. (3). The coherence length of the light source can be determined by comparing the width of the interference profile with the fringe periods. They are found to be $\delta_R = 5.8$ μm, $\delta_G = 4.8$ μm, and $\delta_B = 4.0$ μm for the three red, green, and blue LED's, respectively. The normalized spectra and the interference profiles of the LED's are shown in Fig. 3. The center wavelengths of the LED's are $\lambda_R = 638.4$ nm, $\lambda_G = 528.5$ nm, and $\lambda_B = 457.4$ nm, while the spectral widths are $\Delta_R = 22.9$ nm, $\Delta_G = 33.2$ nm, and $\Delta_B = 28.6$ nm. The measured coherence lengths δ are consistent with the expected values of $(2\ln 2/\pi)\lambda^2/\Delta$ within a factor of 1.3.

#5639 - $15.00 US Received 3 November 2004; revised 14 December 2004; 16 December 2004

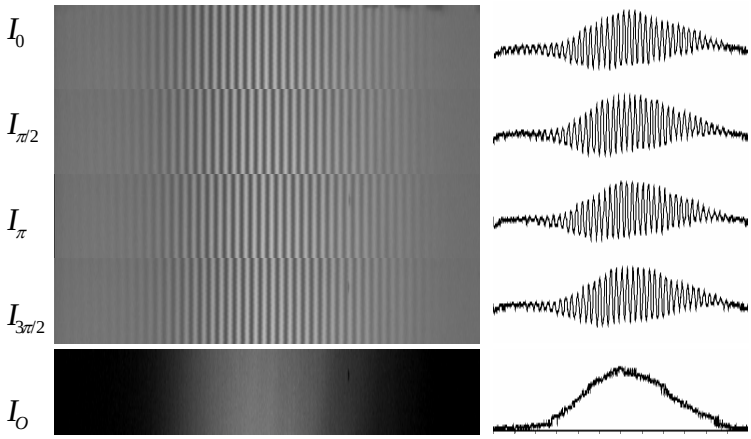

Fig. 2. Phase-shift interference imaging. Four quadrature phase interferograms and the extracted interference images are shown, as well as cross-sectional profiles of the interferograms.

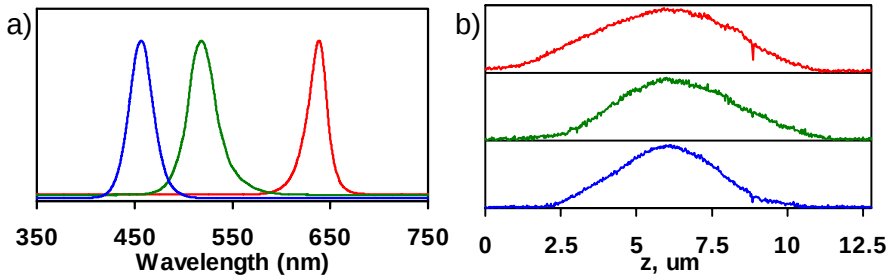

Fig. 3. (a) The spectra of red, green, and blue LED's. (b) The interference profiles of the LED's vs. the axial distance z.

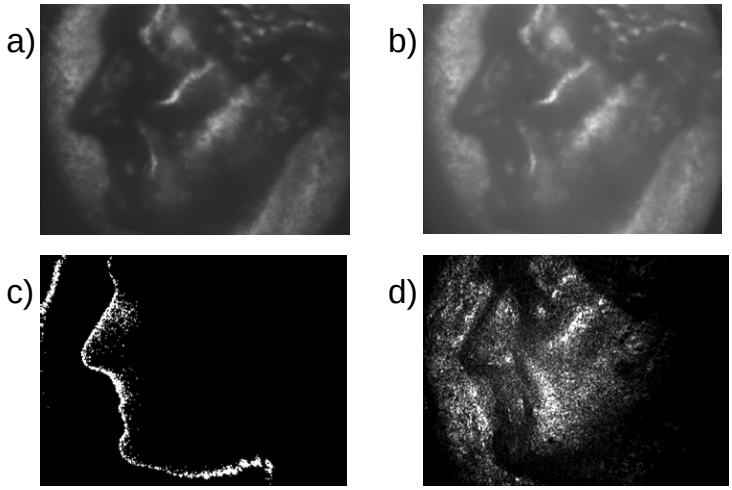

Fig. 4: Phase-shift interference imaging of a coin surface: (a) direct image of the object; (b) image of the object with reference wave; (c) contour image extracted by the phase-shift interference; (d) flat view of the accumulated contour images. (image volume = 12 mm x 9 mm x 405 μm; voxels = 640 x 480 x 82; voxel volume = 19 μm x 19 μm x 5 μm)

#5639 - $15.00 US
Received 3 November 2004; revised 14 December 2004; 16 December 2004

Figure 4 illustrates the WFOCT by phase-shifting interferometry using a coin surface as the test object. Fig. 4(a) is the direct image of the object in the absence of the reference wave, while Fig. 4(b) is when the reference wave is present. Although the two images are mostly indistinguishable, one can observe fluctuating speckles in portions of the object when the camera image is viewed in real time while the reference mirror is dithered. The coherent portion of the image is extracted as described above to obtain a contour of the object at a height that corresponds to the reference mirror position, as shown in Fig. 4(c). We repeat the contour imaging for a number of times (~40) and average to improve the signal-to-noise ratio. The three dimensional imaging is completed by stepping the object z-position over a desired range to obtain a stack of the contour images. The three-dimensional image can then be presented in a number of different ways. In Fig. 4 d) all the contour images are added together resulting in a 'flat view', where all the image planes are in focus and additionally the overall haze in Fig. 4(a) or 4(b) due to stray reflections from various optical surfaces has been removed.

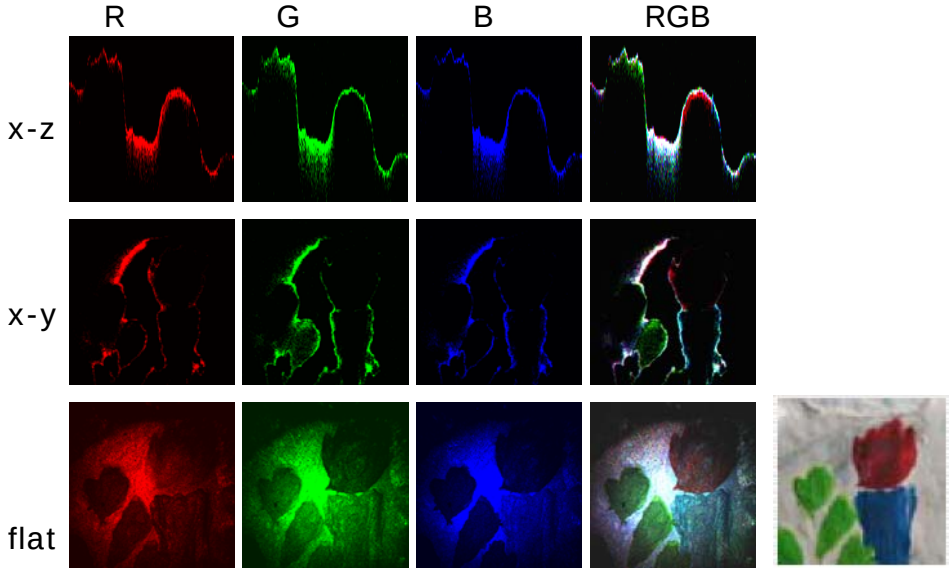

Fig. 5. Color WFOCT of a painted coin surface. See text for details

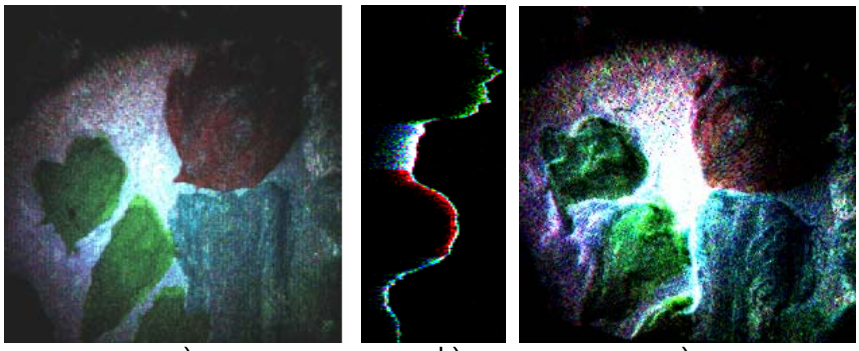

Fig. 6. Color WFOCT movies of a painted coin surface: (a) (1.17MB) xy-section images; (b) (0.26MB) xz-section images; (c) (0.90MB) 3D perspective views. (image volume = 7.2 mm x 7.2 mm x 335 μm; voxels = 480 x 480 x 67; voxel volume = 15 μm x 15 μm x 5 μm)

#5639 - $15.00 US
Received 3 November 2004; revised 14 December 2004; 16 December 2004

For generation of color images, the WFOCT procedure is repeated three times by using red, green, and blue LED's. Each of these generates a three-dimensional image of the object under the respective color illumination. The three 3D images are then combined as RGB channels to generate the final 3D image with full natural color representation of the volume. In Fig. 5, we use a colored coin as the test object. The back side of a dime is painted with red, green, and blue ink and the background is painted white. The first three columns represent separate results obtained using the three LED's. In each column, the top square is a 7.2 mm x 335 μm xz-section view of the 3D image (through a horizontal line near the middle of the field of view) the middle square is a 7.2 mm x 7.2 mm xy-section or a contour image, while the bottom square is the flat view for the color channel. The last column is the (a) is a series of xy-sections and Fig. 6(b) is a series of xz-sections. In Fig. 6(c) the reconstructed 3D image is viewed from varying perspective angles. Notice the strong color-independent (white) reflection at the air-paint interface and strong colored reflection from underneath. Penetration depth in some areas is at least about 100 μm. In the x-z RGB image, top right corner of Fig. 5, the thin and abrupt layer of red probably accounts for thin layer of paint on the metal surface, whereas there is a pool of white paint in the valley next to it. Also note that the RGB flat image, has very respectable color and image quality, compared to the direct photographic image in the lower right corner of Fig. 5.

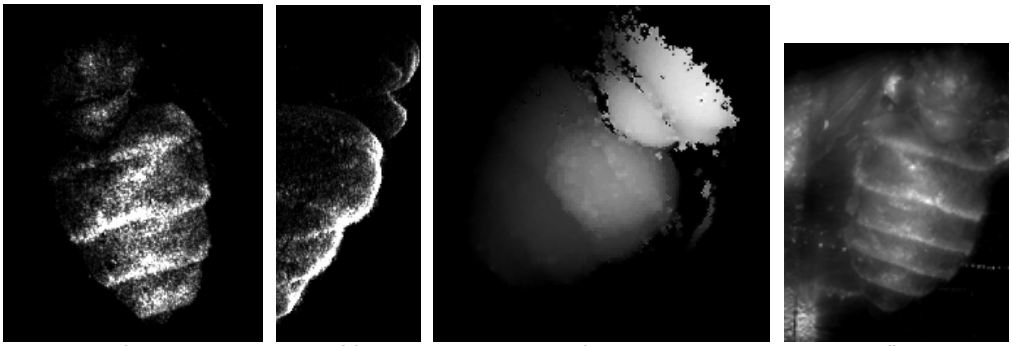

Fig. 7. Monochrome WFOCT movies of a bee: (a) (0.73MB) xy-section images; (b) (0.26MB) xz-section images; (c) (0.64MB) 3D perspective views; (d) direct image of the specimen. (image volume = 6.0 mm x 7.8 mm x 980 μm; voxels = 400 x 520 x 99; voxel volume = 15 μm x 15 μm x 10 μm)

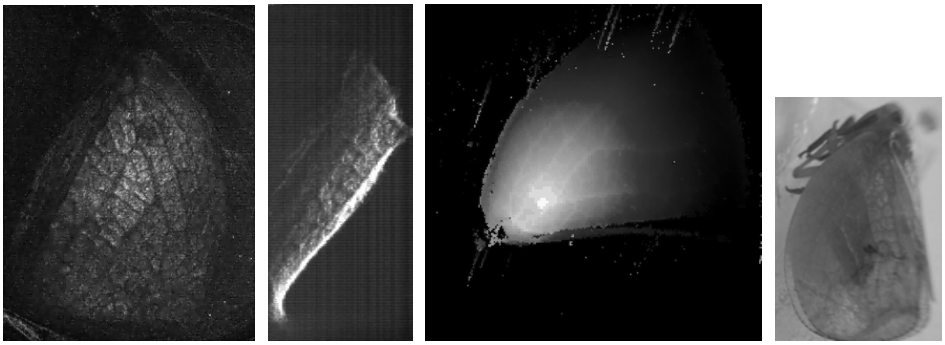

Fig. 8. Color WFOCT movies of an insect wing: (a) (0.81MB) xy-section images; (b) (0.38MB) xz-section images; (c) (0.78MB) 3D perspective views; (d) direct image of the specimen. (image volume = 7.2 mm x 9.6 mm x 810 μm; voxels = 480 x 640 x 82; voxel volume = 15 μm x 15 μm x 10 μm)

#5639 - $15.00 US Received 3 November 2004; revised 14 December 2004; 16 December 2004

3. Biological imaging by WFOCT

Two examples of biological imaging by monochrome WFOCT are shown in Figs. 7 and 8. Figure 7 is the body of a bee and Fig. 8 the wing of an unidentified insect. The XY- and XZ-section movies start with the flat view followed by a series of cross-sectional tomographic views in the respective directions. The image volumes are several millimeters in the lateral direction and less than a millimeter in the longitudinal direction. The relatively opaque body of the bee is seen to have a penetration depth of about 100 μm or so, whereas it is a few hundred microns for the more transparent wing. We have measured the typical signal to noise ratio of these images to be 50 ~ 60 db.

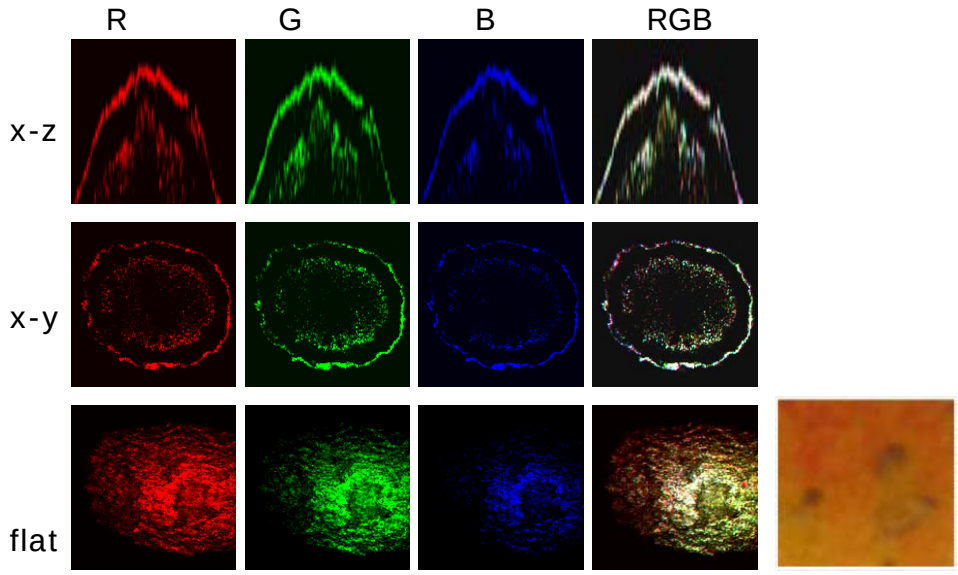

Fig. 9. Color WFOCT of a piece of apple skin. See text for details

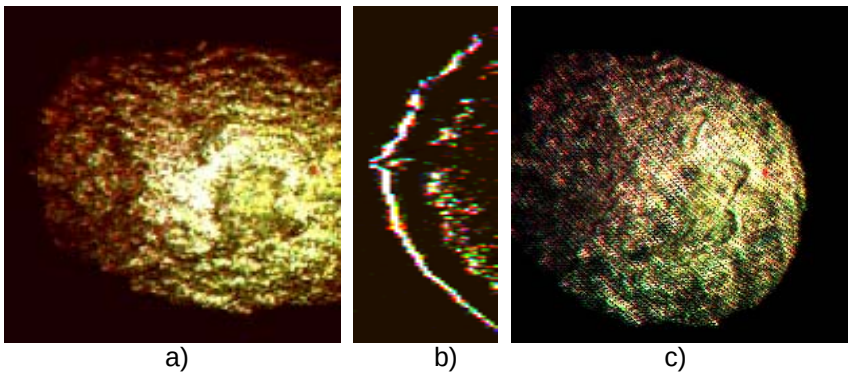

Fig. 10. Color WFOCT movies of apple skin: (a) (0.27MB) xy-section images; (b) (0.10MB) xz-section images; (c) (1.90MB) 3D perspective views. (image volume = 4.7 mm x 4.7 mm x 170 μm; voxels = 313 x 313 x 34; voxel volume = 15 μm x 15 μm x 5 μm)

Next we present examples of color 3D microscopy using the three-channel WFOCT. Figure 9 is arranged in the same manner as Fig. 5, with the XZ- and XY-sectional views and the flat view for each of the three color channels and the RGB composite color images, for a 4.7 mm x 4.7 mm x 170 μm volume of a piece of apple skin. Here the penetration depth is at

#5639 - $15.00 US Received 3 November 2004; revised 14 December 2004; 16 December 2004

least 150 μm, and it displays details of the top surface and the skin tissue. Because of the large difference in the longitudinal and lateral scales, the minute surface texture is seen greatly exaggerated in the flat views. The cross sectional views clearly show the outer skin layer and a portion of the internal tissue layers. One can also notice the correspondence of the internal structure of a blemish area in the x-z sections and flat view images. The extra picture in the lower right corner is a direct photograph of the approximate area of the imaging experiment. Although the color variation of the apple skin is rather subtle and continuous compared to the colored coin experiment, the RGB flat view reproduces the color variation at least approximately. In this data set the colored images are not as one would expect from common macroscopic views of an apple skin. However, under microscope, the coloring of apple skin appears not as a solid layer of red surface, but the red pigments are embedded as numerous particles in otherwise colorless matrix. Still one observes some variation of color that can be attributed to the actual color variation of the surface. Figure 10 presents the movies for XY- and XZ-sections and the 3D images of the data set.

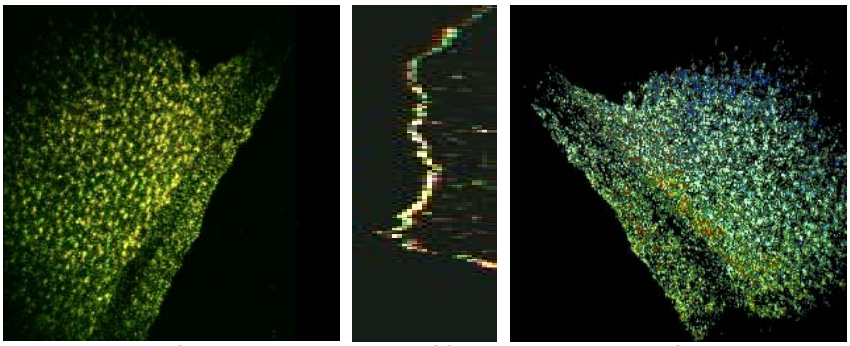

Fig. 11. Color WFOCT movies of a leaf: (a) (0.48MB) xy-section images; (b) (0.15MB) xz-section images; (c) (0.92MB) 3D perspective views. (image volume = 6.3 mm x 6.3 mm x 145 μm; voxels = 420 x 420 x 30; voxel volume = 15 μm x 15 μm x 5 μm)

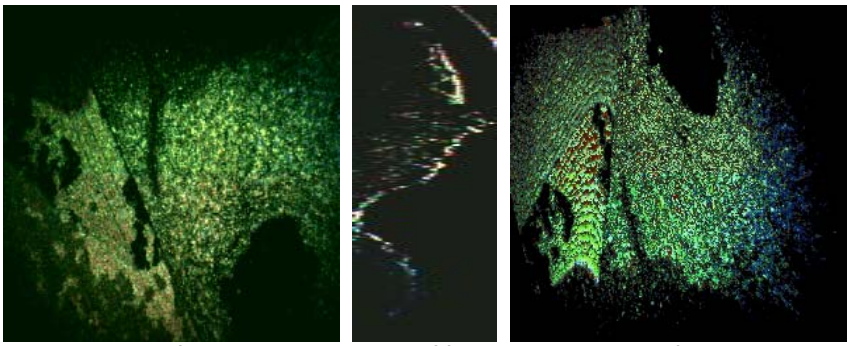

Fig. 12. Color WFOCT movies of a leaf: (a) (0.65MB) xy-section images; (b) (0.22MB) xz-section images; (c) (0.93MB) 3D perspective views. (image volume = 7.2 mm x 7.2 mm x 190 μm; voxels = 480 x 640 x 39; voxel volume = 15 μm x 15 μm x 5 μm)

In Figs. 11 and 12, the color WFOCT is used to generate color 3D images of plant leaves. In Fig. 11, one clearly sees the pattern of pores on the surface as well as a minor stem. A careful examination of the interior of the leaf also shows a fibrous structure running the length of the leaf. In Fig. 12, a piece of scotch tape was present over a part of the leaf in the imaged

#5639 - $15.00 US Received 3 November 2004; revised 14 December 2004; 16 December 2004

area. The 3D imaging system clearly imaged through this slightly diffusing layer. This example also had higher signal level from interior of the leaf tissue. Some of the coloration in these examples is due to various noise in the system, such as color channel misregistration and uncompensated dispersion. Still, given the simplicity of the apparatus used in these preliminary experiments, the overall quality of the images is quite convincing in terms of the resolution, signal level, and the overall capability to generate 3D images with close to natural color information.

4. Discussions and conclusion

In summary, we have proposed and demonstrated a method to generate three-dimensional microscopic images with natural color representation. Using a simple apparatus, we were able to generate images of biological specimens with about 10 μm axial resolution, about 100 ~ 200 μm penetration depth, and 50 ~ 60 db dynamic range. These images are generated with close to natural color representation. One of the technical issues that we plan to address in the future work is to increase the overall efficiency by using a white light illumination with color camera, so that all three color channels can be acquired simultaneously and to process them separately post-acquisition followed by the RGB composition. This would solve the technical difficulty of re-positioning of the separate LED's for the three channels, which apparently contributed to the overall noise of the images. Specifically, the slight misalignment and the difference of illumination patterns of the LED's for the three exposures have the effect of non-uniform or unbalanced illumination among the color channels, although this does not affect the interferometric determination of the object voxel positions. Another improvement is to apply the lock-in detection principle to the image acquisition. The camera frame rate of 30 Hz is too slow for lock-in detection, and instead both the illumination and the reference phase are modulated at a high frequency, say 30 kHz. The phase modulation amplitude is 2π and the illumination is stroboscopically synchronized for one quarter of the period. Accumulation of the image on the CCD effectively provides the low-pass filtering. The process is repeated for four quadrature phases and the resulting four frames of images are to be combined as described above.

Optical section (or tomographic) imaging and imaging through turbid media are very active areas of current research. The proposed method of full color WFOCT microscopy can be used for generating optical section images in a wide range of fields of study including biology, medicine, geology, materials science, and microelectronics. Optical sectioning or tomographic capabilities allow generation of images with entire 3D volume of object sharply in focus. The color imaging techniques provide additional critical information in many of these application areas. Some of the foreseeable applications in biomedicine will be in the imaging of the eyes, the optical biopsy of external tissues, and epithelial layers of gastrointestinal and pulmonary tissues.

Acknowledgments

This work is supported in part by the National Science Foundation.

#5639 - $15.00 US Received 3 November 2004; revised 14 December 2004; 16 December 2004